

1 Observations of Hydrography and Downflow of
2 Brine-enriched Shelf Water in the Storfjorden
3 Polynya, Svalbard

R. Skogseth¹, L. H. Smedsrud², F. Nilsen^{1, 3}, and I. Fer^{3, 2}

R. Skogseth, Department of Arctic Geophysics, The University Centre in Svalbard (UNIS),
P.O. Box 156, N-9171 Longyearbyen, Norway. (ragnheid.skogseth@unis.no)

¹Department of Arctic Geophysics, The
University Centre in Svalbard (UNIS),
Longyearbyen, Svalbard, Norway

²Bjerknes Centre for Climate Research,
Bergen, Norway

³Geophysical Institute, University of
Bergen, Norway

4 **Abstract.** Observations of hydrography and currents in the active Stor-
5 fjorden polynya during field work in April 2004 and 2006 are presented. The
6 polynya adds salt from its efficient ice production, usually increasing the den-
7 sity $\sim 0.15 \text{ kgm}^{-3}$. Downflow of dense water from the coastal polynya to the
8 deeper basin enclosed by the Storfjorden sill was captured in both years. April
9 2006 had a period of strong heat loss and intense frazil ice growth in the polynya.
10 This created downflow of brine-enriched shelf water (BSW) with a maximum
11 salinity of 35.25, i.e. an increased density $\sim 0.4 \text{ kgm}^{-3}$ above that of the source
12 water. In April 2004, the salinity remained lower than BSW ($S > 34.8$), re-
13 flecting the fresh source water in fall 2003 due to the heavy ice conditions
14 in the western Barents Sea that year. A portion (0.05 Sv) of such source wa-
15 ter probably enters Storfjorden through Freemansundet where the mean cur-
16 rent transports less saline and warmer water from the northwestern Barents
17 Sea. Freemansundet has additionally a strong tidal current peaking at 53 cms^{-1} ,
18 dominated by the M_2 component. The tidal wave propagates through the
19 narrow sound producing shallow water components and a locally well mixed
20 water column. The estimated ice production in winter 2004, twice as large
21 as that of winter 2006, could not overcome this less saline well mixed source
22 water. BSW downflow within Storfjorden was both observed and modeled
23 to occur in areas with steep bathymetry. Our observations show that high
24 resolution hydrographical data, spacing less than 0.5 km, are necessary to
25 resolve such downflow. Consistent with the observed polynya water salinity,
26 current data at the sill showed weaker overflow in 2004 than in 2006. Over-

27 flow of BSW was observed on the eastern part of the Storfjorden sill in April
28 2006, indicating that overflow occurs across the entire sill width during the
29 freezing period. Current, temperature and salinity data from the overflow
30 indicate a time lag of 12-18 days between the BSW production and the sill.
31 This downflow-overflow link is confirmed by a numerical experiment and an-
32 alytical scaling, making results applicable to other polynyas.

1. Introduction

33 The Arctic continental shelves are sites for active water mass transformations in winter,
34 particularly in their coastal polynyas. Polynyas are persistent and durable ice-free areas
35 in otherwise ice-covered waters, and are formed and maintained by offshore winds, tides
36 and currents advecting the ice away from the coast (latent heat polynya) or by upwelling
37 warm water melting the ice cover (sensible heat polynya). Intense heat loss from the open
38 water to the atmosphere leads to rapid and persistent ice growth in latent heat polynyas.
39 Brine rejected from growing sea ice forms dense, brine-enriched shelf waters (BSW) that
40 accumulate near the bottom of shelf basins and eventually spill towards the deep sea as
41 dense plumes. Plumes originated from BSW are climatically important as they contribute
42 to ocean stratification in the Arctic [Aagaard et al., 1981] and may ventilate the Arctic at
43 a rate comparable to open ocean convection [Rudels and Quadfasel, 1991; Cavalieri and
44 Martin, 1994].

45 The processes controlling the accumulation of BSW in the basins of the continental
46 shelves are, in general, poorly understood, partly owing to their small spatial scales and
47 to extreme climatic conditions. According to model studies [Gawarkiewicz and Chapman,
48 1995], polynya activity and accompanying brine rejection will create density fronts along
49 the polynya edge. Geostrophic currents established along the front lead to baroclinic
50 instability and eddies which generate an across-shelf exchange of BSW from the shallow
51 polynya area to the deeper basin. Yearlong observations of current and water mass trans-
52 formation from moored instruments in coastal polynyas with accompanying satellite and
53 hydrographical data have only been reported for the St. Lawrence Island polynya in the

54 Bering Shelf [Drucker et al., 2003; Danielson et al., 2006] and the Northwestern polynya in
55 the Okhotsk Sea [Shcherbina et al., 2004]. These studies showed that the two shelf areas
56 with different circulation and bathymetry, responded differently to the polynya activity.
57 Despite brine rejection during ice growth and the accompanying BSW formation at both
58 sites, no eddy activity was detected by the 14 moorings in the St. Lawrence polynya
59 [Danielson et al., 2006], whereas eddies due to baroclinic instability were suggested to
60 cause the across-shelf exchange of BSW in the Northwestern polynya [Shcherbina et al.,
61 2004]. Increased knowledge on polynya processes and the ocean response to polynya ac-
62 tivity on continental shelves in marginal seas is crucial to estimate reliable bulk fluxes
63 and to improve sea ice and ocean circulation models.

64 A recurring latent heat polynya is known to form inside Storfjorden during northeasterly
65 winds in winter [Haarpaintner et al., 2001; Skogseth et al., 2004] producing typically 0.03-
66 0.04 Sv of BSW annually [Skogseth et al., 2004, 2005a]. A sill at the mouth of Storfjorden
67 separates dense basin water from the adjacent shelf areas. We refer to BSW flow from
68 shallow polynya to deeper part of the basin as "downflow" and that across the sill as
69 "overflow".

70 Plumes of dense water originating at the Storfjorden polynya have been frequently ob-
71 served south of the sill towards the shelf break of the West Spitsbergen Shelf [Quadfasel
72 et al., 1988; Anderson et al., 1988; Schauer, 1995; Schauer and Fahrback, 1999; Fer et al.,
73 2003, 2004b; Fer, 2006]. If its density excess permits, the plume cascades into the deep
74 Norwegian Sea and northward along the eastern slope of Fram Strait towards the Arctic
75 Ocean [Quadfasel et al., 1988]. Despite relatively constant BSW volume flux from the
76 polynya, the maximum observed BSW salinity varies interannually by more than unity

77 [Skogseth et al., 2005b]. The density of the overflow varies accordingly, affecting the
78 penetration depth of the plume. The motivation of this study is to better understand
79 the exchange between the polynya and the Storfjorden basin, the downflow of BSW and
80 polynya dynamics-overflow relations and to generalize the results for other polynya sys-
81 tems.

82 As a part of the Polar Ocean Climate Processes (ProClim) project a fieldwork pro-
83 gram was conducted in the Storfjorden polynya in April 2004 and 2006 to study the ice
84 properties and processes inside a polynya, and the ocean response to polynya activity.
85 Observations from 2004 on properties of grease and thin ice were presented in Smedsrud
86 and Skogseth [2006], and results from 2006 focusing on heat flux, frazil ice growth and
87 supercooling in Skogseth et al. [2007a]. In this paper, we present observations of the ocean
88 response to an active polynya, documenting rapid water transformation. Conditions dur-
89 ing field experiments are described in Section 2. Results in Section 3 describe wind and
90 tidal influence on the source water for BSW production in the polynya, as well as areas for
91 downflow, controlling mechanisms, and time scales on the downflow-overflow connection.
92 Interannual variability and effects of topography and eddies on downflow are discussed in
93 Section 4. A numerical experiment confirms downflow sites of BSW as well as the link
94 and time delay between water transformation in the polynya, downflow and overflow at
95 the sill. We conclude our findings in Section 5.

2. Environmental Conditions and Sampling

2.1. Storfjorden Polynya Overview

96 Located on the eastern side of Svalbard, Storfjorden (Figure 1) is largely isolated from
97 the heat transported towards the Arctic by the North Atlantic Current. The fjord is

98 generally ice covered from December through June. The processes taking place here are
99 in many ways representative of those in the Arctic shelf seas. Storfjorden has large shallow
100 areas where the temperature in winter is at the freezing point over the entire water column,
101 and further heat loss leads to ice production and brine release and increase the bottom
102 salinity. Variations in atmospheric forcing over the polynya brings significant differences
103 between winters and their sea ice cover. An analytical polynya model [Skogseth et al.,
104 2004] driven by atmospheric observations and partially validated by remote sensing data,
105 gives a mean winter ice production between 1998-2001 of 40 km^3 over a mean polynya
106 area of $48 \times 60 \text{ km}^2$. Compared to this, ice production in 2004 and 2006 was above (48.4
107 km^3) and below (24.9 km^3) the average, respectively

108 This variability was caused by a more frequent wind in direction favoring polynya open-
109 ing (Figure 2a) and a larger net heat loss to the atmosphere (Figure 2b) in 2004 compared
110 to 2006. The main wind driven polynya activity did not start until February in 2006,
111 whereas the winter season 2004 had an active polynya opening period from December
112 2003 until March 2004. A steep rise in the cumulative sum of the wind component fa-
113 vorable for ice transport out of Storfjorden (φ_0) in March 2006, combined with steep rise
114 in the cumulative sum of net heat exchange, reflect the intense ice production and water
115 mass transformation observed this month. The heat loss to the atmosphere during the
116 winter season 2006 is less than that in 2004, owing to frequent (above normal) southerly
117 wind periods bringing warm air over Svalbard. The dominance of southerly winds is also
118 seen by the wind component in Figure 2a showing a negative trend in the cumulative sum
119 from the end of December until the beginning of February 2006, a period with none or
120 very little polynya activity.

121 March and April usually have comparable and significant total ice growth of 5-10 km³
122 [Skogseth et al., 2004], but the contribution from May is quite small. The polynya area
123 (open water and thin ice) changes quickly through the winter mostly due to the changing
124 polynya width, which may increase with ~ 80 km over a few days due to northerly winds
125 [Smedsrud et al., 2006]. Conditions during our experiments in 2004 and 2006 were thus
126 typical covering a large polynya and intense freezing, to a small and closing one with nearly
127 no freezing at all. Field experiments conducted in April 2004 and 2006 are described
128 separately in the following.

2.2. Experimental methods

129 All CTD profiles (Figure 1) were obtained by a SeaBird Electronics SBE19 (unpumped)
130 sonde. The sensor suite was lowered and heaved at a speed in the range of 0.3-1.0 ms⁻¹,
131 and the temperature (T) and conductivity (C) sensors were aligned in advance to pressure
132 (P) according to the descent rate of each cast. The accuracy is 0.14 dbar for P, 0.005
133 °C for T and 0.0005 Sm⁻¹ for C. The CTD data are corrected against 15 and 11 water
134 samples taken in 2004 and 2006, respectively, from a 1.7 litres Niskin bottle. The resulting
135 uncertainty of the derived salinity is estimated to be 0.01. In order to avoid freezing of
136 the sensors between stations, the CTD was kept in a heated box together with the Niskin
137 bottle and the water sample bottles. The CTD sonde was first lowered to and maintained
138 at 5-10 m depth until the measurements stabilized, then it was heaved to just below the
139 surface ready for profiling. Both down- and up-casts were recorded.

2.3. April 2004

140 Hydrographic observations were made close to Kapp Lee in the Storfjorden polynya
141 (Figure 1), between April 16 and 24 2004. In total, 15 CTD stations were occupied from
142 the fast ice edge along the polynya and through holes in the fast ice in Freemansundet
143 accessed by a snowmobile.

144 For the duration of the experiment, the Storfjorden polynya consisted of mostly open
145 water and some thin ice. Satellite inferred ice-chart shows the open water in Storfjorden
146 two days prior to the field work (Figure 3a). The wind, recorded on Hopen Island, was
147 from the north and northeast advecting the pack ice away from the fast ice in northern
148 Storfjorden and along the west coast of Edgeøya. This resulted in a confined polynya
149 edge along the fast ice border on the upwind end of the polynya, and a relatively diffuse
150 polynya border on the downwind end towards the pack ice. During the field work period,
151 the wind gradually turned southeasterly, closing the polynya with growing thin ice and
152 pack ice, despite the increasing air temperature from -20°C towards 0°C .

153 The hydrographic observations were supplemented by current measurements recorded
154 by an Aanderaa Instruments Recording Doppler Current Profiler (RDCP). The RDCP
155 was deployed in the under-ice boundary layer in Freemansundet, at $78^{\circ} 07.348' \text{ N}$ and 020°
156 $49.001' \text{ E}$ (Figure 1) and acquired data from April 18 2004 1600 UTC to April 21 2004
157 2200 UTC covering approximately 6.5 semi-diurnal cycles. Profiles from the downward-
158 looking RDCP were collected at 2 m depth bins with the first bin approximately 3.6
159 m below 1.2 m of fast ice, in a 32 m deep water column. Three-dimensional currents
160 were averaged every 10 minutes. An additional conductivity sensor on RDCP provided

161 salinity measurements with an uncertainty of about ± 0.08 psu after calibration against
162 CTD observations and water bottle samples.

2.4. April 2006

163 Hydrographic observations in 2006 covered both the polynya region and the Storfjorden
164 sill at 77° N (Figure 1). In total, 21 polynya stations were occupied from the fast ice
165 edge close to shore at Kapp Lee and from a small fibreglass boat deployed in the polynya.
166 The sill region was accessed by the icebreaker K/V Svalbard and 24 additional CTD casts
167 were made between April 21 and 23 in the vicinity of the sill.

168 Ice conditions during the 2006 experiment were significantly different than in 2004. Fast
169 ice was absent in Storfjorden. Figure 3b) shows the ice conditions in the middle of the
170 7 days of polynya field work, after the wind direction turned from northeast to east on
171 April 3. Prior to the event the polynya was open and intense frazil ice growth occurred.
172 After April 3, the air temperature increased and frazil ice growth ceased. The polynya
173 gradually closed, however, a patch of open water remained in the vicinity of Kapp Lee on
174 Edgeøya (Figure 1). During the cruise with K/V Svalbard, the pack ice was very compact
175 inside Storfjorden. The ice conditions shown 3 days before the cruise start (Figure 3c)
176 persisted throughout the cruise. The ice pack increased in thickness towards the north,
177 and CTD measurements were made in an area with ~ 3 m rubble ice as far north as the
178 vessel could access.

179 Supplementary data consisting of current profiles and bottom T/S time series are avail-
180 able through a monitoring programme at the Storfjorden sill. Current profiles are acquired
181 by an upward-looking 300 kHz broadband Workhorse, RD Instruments Acoustic Doppler
182 Current Profiler (ADCP) deployed at the sill ($76^\circ 58.08'$ N, $019^\circ 14.95'$ E, Figure 1) av-

183 eraging 10 minute ensembles at 4 m vertical bins. The first bin was centered at about 6
184 m above the bottom. The bottom frame was equipped with a SBE37 Microcat, approxi-
185 mately 0.5 m above the bottom, recording bottom T/S every 10 minutes. The Microcat
186 derived salinity was corrected against available CTD casts collected at several occasions.

3. Results

3.1. Polynya

187 Polynya waters are characterized by high-salinity dense water at freezing point tem-
188 perature. A composite potential temperature (θ), salinity (S) diagram of all CTD data
189 collected during both field experiments exemplify the winter-time water mass transfor-
190 mations in Storfjorden (Figure 4). Early into the experiment in April 2006, atmospheric
191 conditions favored polynya activity, frazil ice growth and brine release. During the first
192 three days, the polynya water was supercooled with salinity reaching 35.9. Following this
193 event, the maximum salinity observed, $S=35.25$, is about 0.6 higher than that in April
194 2004. Bottom-attached, polynya-origin water is detected in the casts made in the vicinity
195 of the Storfjorden sill in late April 2006 (Section 3.2). Diapycnal mixing lines can be
196 recognized in the θS diagram (Figure 4) between polynya (or polynya origin) water and
197 relatively warmer, less saline ambient water, both in the polynya area and at the sill,
198 approximately 120 km downstream (Section 3.2).

199 Isopycnals derived from the section worked in 2004 along the fast ice edge, on the
200 upwind side of the polynya, show evidence of dense water (σ_θ ca. 27.86 kgm^{-3}) downflow
201 from the shallows (Figure 5). Denser polynya water, observed in the deeper part of the
202 section, is likely convected in a similar manner from the polynya, prior to the experiment.
203 Comparable downflow events are observed in April 2006. Figure 6 shows the sections

204 of isopycnals obtained in the polynya, 4 days after the supercooling event. Of the two
205 sections worked from the shallows near Kapp Lee towards the deeper basin (Figure 6a-
206 b), the section joining Stations 13-6 has the densest polynya water ($\sigma_\theta=28.32 \text{ kgm}^{-3}$)
207 spilling down the steep bathymetry. However, both sections show patches of polynya
208 water, suggesting sluggish downflow in response to polynya activity. The doming of the
209 isopycnals between Stations 8 and 10 (Figure 6b) suggests an eddy-like feature. The
210 section approximately along the 30-m isobath shows the densification towards the polynya
211 (Figure 6c).

212 The shallow Storfjordbanken south of Edgeøya is another candidate polynya site that
213 could supply dense water into the basin. Figure 7 shows isopycnals along a section fol-
214 lowing the 60-80 m isobaths at the western flank of Storfjordbanken. Here, near bottom
215 density is about 0.4 kgm^{-3} less than that in the polynya, and downflow of dense water
216 from the bank toward the deep trough is not detected. Instead, a north-south density gra-
217 dient is recorded across the mouth of the fjord, with water in the basin being denser than
218 that south of the sill. The sharpest density front is located in the upper 30 m between
219 Stations 37 and 36.

3.2. Sill

220 The CTD section obtained in the vicinity of the sill in late April 2006 shows a $\sim 30 \text{ m}$
221 thick overflow of dense water between Stations 51 and 48 at the eastern part of the sill
222 (Figure 8). Here, the plume has salinity up to 35.2 and temperature down to $-1.95 \text{ }^\circ\text{C}$. An
223 equally thick layer of dense bottom-attached plume is present in the hollow southeast of
224 the sill, between Stations 47 and 42. Hydrographic properties cover a wider range near the
225 sill compared to the polynya. Additional isopycnal mixing lines and intrusive features can

226 be seen between warmer ambient water above the plume at the sill and cold Storfjorden
227 water in the basin (Figure 4).

228 Time series of current profiles at the sill (Figure 1) together with the bottom tempera-
229 ture and salinity show a saline plume near freezing temperature flowing past the mooring
230 site (Figure 9). Bottom salinity gradually increases through mid-March and mid-April.
231 Cross-sill component of the velocity is bottom-enhanced, reaches 20 cms^{-1} and occasion-
232 ally extends over 60 m from the bottom. Pulsing events associated with high bottom
233 salinity are likely linked to strong polynya activity and supercooling events.

3.3. Tides and Currents in Freemansundet

234 The polynya is in close proximity to Freemansundet, characterized by strong currents
235 and tides. This influences the polynya dynamics and water mass properties, through
236 both mixing and advection. Time series of nearly full-depth current profiles are analyzed
237 with emphasize on tides and residual currents. There is a nearly barotropic total current
238 through the sound with amplitude reaching 53 cms^{-1} . The tidal ellipses for the most sig-
239 nificant constituents, derived using the harmonic analysis of the barotropic and baroclinic
240 time series [Pawlowicz et al., 2002] are shown in Figure 11. The dominant constituent is
241 the semi-diurnal M_2 with maximum total (barotropic and baroclinic) amplitudes up to
242 47 cms^{-1} at 26 m depth. The M_2 tidal wave is nearly rectilinear along the sound axis
243 with marginal clockwise rotation. The higher tidal harmonics M_4 and M_6 are significant
244 with total amplitudes up to, respectively, 3.5 cms^{-1} and 4.5 cms^{-1} at 26 m depth. While
245 the ellipse of the M_6 tide behave like the M_2 constituent, that of M_4 is aligned in a more
246 east-west direction (Figure 11). Furthermore, M_4 is the least unidirectional and the ro-

247 tation of the baroclinic ellipses becomes increasingly clockwise (counterclockwise) as the
 248 ice (bottom boundary) is approached.

249 Residual currents obtained by time averaging 25 h low-passed horizontal velocity com-
 250 ponents are directed into Storfjorden at all depths (Figure 12). The mean residual current
 251 varies between 2.4 cms^{-1} (at 20 m) and 1.5 cms^{-1} (at 8 m), comparable to M_4 , M_6 and
 252 K_1 constituents. The mean residual current vectors rotate counterclockwise (clockwise)
 253 with depth above (below) about 18 m, suggesting boundary layers towards the ice-water
 254 interface and the bottom. The width of Freemansundet, at the current measurement site,
 255 is approximately 8 km with a mean depth of about 30 m. Using the depth averaged
 256 residual current of 2.0 cms^{-1} , the net transport through the sound during the measur-
 257 ing period is estimated to be 0.05 Sv, directed into Storfjorden. This is comparable to
 258 the typical annual BSW production in Storfjorden polynya, and approximately half the
 259 annual overflow volume transport estimates at the sill.

4. Discussion

4.1. Interannual Variability

260 Observations show large differences between April 2004 and 2006 hydrography (Figure
 261 4). In April 2004, the salinity of the polynya water close to Kapp Lee was less than 34.7.
 262 This is by definition not BSW ($S > 34.8$ and $T < -1.5 \text{ }^\circ\text{C}$, [Schauer, 1995]). In April 2006,
 263 the maximum salinity of the polynya water close to Kapp Lee was 35.9 during frazil ice
 264 growth in supercooled water [Skogseth et al., 2007b] and was 35.25 under atmospheric
 265 conditions comparable to April 2004. The overflow salinity at the sill was ~ 35.2 in April
 266 2006. Observations in Storfjorden reveal annual maximum BSW salinity of $S = 35.20 \pm 0.26$

267 (\pm one std) when averaged over 1981 to 2002 [Skogseth et al., 2005a, b]. The brine
268 production in 2004 is thus poor, and that in 2006 is moderate.

269 The BSW production and its interannual variability in the polynya have consequences
270 for the overflow strength and its variability at the sill (Section 4.4). Mean profiles of the
271 cross-sill velocity measured by the ADCP at the sill (Figure 10) show weaker overflow in
272 April 2004 than that in 2006. This is consistent with the observations in the polynya, the
273 inferred interannual variability and the strength of the BSW production.

274 The low salinity of the polynya water in 2004 might be explained by the ice conditions in
275 western Barents Sea the preceding spring/summer. In the period 1998 to 2006, 2003 was
276 the only year when the winter ice condition in Storfjorden and western Barents Sea was
277 characterized by a dense ice cover comprising multi-year ice [Haas et al., 2004]. Satellite
278 derived ice motion and thickness records from 1994 to 2003 indicate that in 2003 an
279 unusual large ice volume flux occurred through the Svalbard-Franz Josef Land passage
280 into the Barents Sea [Kwok et al., 2005]. This is probably the main reason for the heavy ice
281 conditions in Storfjorden and western Barents Sea in 2003. The ice extent in the Barents
282 Sea correlates with the surface layer salinity in the Barents Sea the following autumn
283 due to the freshwater supply from melting sea ice [Maus, 2003]. The large amount of ice
284 in 2003 then resulted in a relatively less saline surface layer in Storfjorden and western
285 Barents Sea the following autumn. Hence in 2004, more ice formation was necessary to
286 transform the polynya water into BSW [Skogseth et al., 2004, 2005b].

287 The ice production in Storfjorden was estimated to be 48 km^3 in winter 2004, the second
288 largest since winter 1998 [Skogseth et al., 2005a]. This was still not enough to transfer the
289 surface water to BSW. Even though not BSW by definition, polynya processes in 2004

290 densified the shallows near Kapp Lee. The downflowing plume in Figure 5 is 0.1 kgm^{-3}
291 denser than the ambient and most likely a consequence of a freezing event prior to the
292 April 2004 section.

4.2. Tidal Currents and the Polynya

293 As opposed to the interannual variability of the atmosphere, tides have a constant ef-
294 fect on the polynya, and play an important part in mixing the source waters. The near
295 barotropic total current in Freemansundet was tidally dominated. The semi-diurnal con-
296 stituent M_2 explained $\sim 98\%$ of the barotropic tidal pattern (Figure 11). At this latitude,
297 the semi-diurnal and inertial period motions cannot be separated by the harmonic analysis
298 of such short time series. The M_2 amplitude detected by the harmonic analysis can there-
299 fore be biased large owing to the contribution from the inertial period. The barotropic
300 M_2 ellipse had clockwise rotation with eccentricity close to zero. The current was thus
301 aligned along the Freemansundet axis. Earlier model studies of Storfjorden with proper
302 representation of the two sounds (Freemansundet and Heleysundet) showed significant
303 current owing to a $200^\circ - 220^\circ$ phase shift in the M_2 tide between inner Storfjorden
304 and northwestern Barents Sea which generated a sea surface elevation difference along
305 the sounds [Skogseth et al., 2007b]. The CTD section across the RDCP station in Free-
306 mansundet obtained in April 2004 (not shown, see Figure 1 for station reference) revealed
307 a well-mixed water column throughout the section due to the strong tidal current and
308 corresponding mixing.

309 The shallow water constituents M_4 and M_6 explained a negligible fraction of the
310 barotropic current (Figure 11). These overtides at double and triple the M_2 frequency

311 are nonlinear interaction of M_2 with complex topography when the tidal wave propagates
312 through shallow Freemansundet.

313 The general rotation of the tidal ellipses were clockwise, but some boundary layer effects
314 were seen on the M_4 , M_6 and K_1 tidal ellipses. As the ice-water interface is approached,
315 the baroclinic M_4 and M_6 ellipses became more polarized and dominated by the clockwise
316 rotation and changed sense of rotation and alignment with depth. The baroclinic K_1 tidal
317 ellipse rotated clockwise at all depths, but the orientation was strongly depth-dependant.
318 These effects increased the tidal stirring through the sound and the water stress on the
319 ice. The tidal stress on ice can be crucial for the polynya opening and closing, and can
320 aid wind to break off the fast ice and generate the upwind edge of the polynya. In April
321 2004, the tidal stress through Freemansundet was observed to be strong enough to open
322 and close a 100-200 m wide polynya during calm wind conditions. In the future, the tidal
323 stress should be included in the analytical polynya model in Storfjorden [Skogseth et al.,
324 2004].

325 The residual current (tidal oscillations removed) showed a net transport into Storfjorden
326 through Freemansundet (Figure 12). The residual current veers to the right towards the
327 ice-water interface and the bottom consistent with the boundary layer effects on the
328 baroclinic M_4 , M_6 and K_1 ellipses (Figure 11). Hence, the turning of the residual current
329 with depth probably was a nonlinear effect due to the bathymetry and the jet-like tidal
330 current through the sound.

331 The RDCP measured relatively higher salinity and lower temperature when the total
332 current was directed into northwestern Barents Sea, than when directed into Storfjorden
333 (not shown). Saltier and colder water in inner Storfjorden is likely caused by the polynya

334 and accompanying large heat fluxes, effective frazil ice growth and brine release. The
335 increasing trend in temperature and a slightly decreasing trend in salinity time series (not
336 shown) reflects the direction of the mean residual current, transporting less saline and
337 warmer water from the east. The water mass transformation in Storfjorden thus involves
338 partly the inflowing water above the sill in the south and that through Freemansundet.

4.3. Effects of Topography

339 During winter, the downflow of BSW from the shallow near-shore areas gradually fills
340 Storfjorden to the sill level [Skogseth et al., 2005a, b]. Noticeably, 55% of the Storfjorden
341 area is shallower than 70 m, and 16% of the area is deeper than the sill depth and occupies
342 only 5% of the total volume [Skogseth et al., 2005b]. Although the polynya length (normal
343 to the coast line) is of order 50 km on the average, the densification due to brine production
344 is limited to the shallows with significantly less horizontal extend. Isopycnals for years
345 2004 and 2006 suggest a length scale of order 5 km where a large fraction of the water
346 column is densified and a lateral density gradient is established between the shallows
347 and the adjacent water. It is this lateral density gradient that drives the downflow and
348 flushing of the polynya waters. The effective discharge from the polynya and total volume
349 transport of BSW from the shallows are the sum of flushing events of such length scale
350 over about 50-60 km width (polynya width) along the coast.

351 The mechanisms involved in dense water cascades off the continental shelf, including
352 initiation and development stages of downflow, were described in Shapiro et al. [2003].
353 In the Storfjorden polynya, although the polynya spans isobaths down to 100 m, the
354 ice production and brine rejection are not homogenous, and densification is favored in
355 shallows. The lateral density contrast is either controlled by the ratio of the cumulative

ice production in the shallows to that in deeper portions of the polynya, or if this ratio is close to unity, by the relative difference of the depth of the shallows and the halocline [Shapiro et al., 2003]

In the absence of along-slope gradients and lateral diffusion, and assuming steady state with negligible cross-slope advection in the bottom boundary layer, Shapiro et al. [2003] suggest $R_H = (\Delta\rho\alpha g)/\rho Lf^2 < 1$ for the existence of a steady-state boundary layer solution, and $R_H > 1$ for accelerating events. Here, $\Delta\rho$ is the density difference over the lateral distance L , and α is the bottom slope. In 2006 from Figure 6b, we estimate $R_H > 1$ using $\Delta\rho = 0.08 \text{ kgm}^{-3}$ over 0.8 km and a bottom slope of about 25 m per 0.8 km, suggesting an accelerating downslope event. In 2004 from Figure 5, we estimate $R_H < 1$ using $\Delta\rho = 0.06 \text{ kgm}^{-3}$ over 2 km and a bottom slope of about 30 m per 2 km.

Figures 1 and 6 show that BSW flowed along a channel towards deeper basins (Section 20-26), but that downflow with denser BSW occurred at steeper bathymetry (Section 13-6). Through the depth-contour-following section (Section 20-13), the densest BSW was detected at Station 16 ($78^\circ 04.4' \text{ N}$, $020^\circ 36.3' \text{ E}$), indicating favorable bathymetry for downflow at this site. The distance between the CTD stations in the sections are ~ 0.5 -1 km. Clearly, high-resolution hydrographical sampling and bathymetric maps are needed to resolve and predict the BSW downflow in areas with such complex bathymetry as Storfjorden. Bathymetric data of Storfjorden with a resolution of $0.5 \text{ km} \times 0.5 \text{ km}$ [Skogseth et al., 2005b] should be used in future model studies.

4.4. Downflow-Overflow Link

The polynya activity over shallow areas effectively fills the volume below the sill level with BSW. Skogseth et al. [2005a] infer a typical annual BSW production of about $V_{BSW} =$

378 10^{12} m^3 in the years 1998-2002, i.e. 0.06 Sv over a freezing period of 180 days. Here, we
 379 show that the BSW interface reached the sill level in about 25 days, which was at the
 380 time of the experiment in April 2006. Subsequent events with accompanying downflow
 381 that reach the interface will propagate to the sill in 1 to 3 days.

382 The effective polynya volume is $V_P = hLW = 7.5 \times 10^9 \text{ m}^3$, using a mean polynya
 383 depth $h = 30 \text{ m}$, length $L = 5 \text{ km}$ and width $W = 50 \text{ km}$. During one freezing period,
 384 the polynya flushes $V_{BSW}/V_P \approx 130$ times over a typical freezing period of 180 days. The
 385 buoyancy forcing due to freezing between the polynya flushing events sets the density
 386 anomaly that triggers the subsequent flushing and its time scale $\tau = L/\sqrt{g'h}$ [Fer et al.,
 387 2002], i.e. 7 hours for a typical densification of $\Delta\rho = 0.15 \text{ kgm}^{-3}$. Over 130 flushing
 388 events, this amounts to 20% of the freezing period.

389 In the initial stage of the downflow, before the rotational control is established, the
 390 steady state downslope speed of a plume with thickness h_p is $u = \sqrt{g'h_p(\sin\alpha/C_D)}$ [Fer
 391 et al., 2002]. Using a typical range for the drag coefficient ($C_D = 2 - 5 \times 10^{-3}$), $\Delta\rho = 0.15$
 392 kgm^{-3} , $h_p = 10 \text{ m}$ and a bottom slope of $2 - 5 \times 10^{-3}$, u is in the range of 10-20 cms^{-1} .
 393 Within 12 hours until rotational control is achieved, the plume will sink from the mean
 394 polynya depth to the 38-75 m isobath. Consequently, the rotationally controlled plume
 395 moving along the slope with speed $V_{Nof} = g'\alpha/f = 0.03 - 0.05 \text{ ms}^{-1}$ [Nof, 1983; Wålin,
 396 2004] will gently cross the isobaths due to friction. The descent rate is roughly 1/400
 397 [Killworth, 2001], corresponding to an alongpath distance of 46-60 km, for the 115-152 m
 398 vertical descent to the 190 m deep basin. This translation will be covered within 11-23
 399 days.

400 A conservative estimate of the filling-time for the Storfjorden basin can be obtained
401 using the shortest path (46 km) and $V_{Nof} = 0.05 \text{ ms}^{-1}$. The volume below the sill is
402 $54 \times 10^9 \text{ m}^3$. In the absence of entrainment, the polynya needs to flush the shallows 7
403 times ($54 \times 10^9 / 7.5 \times 10^9$) to fill this volume. The BSW plume will increase in volume
404 due to entrainment along the path. Using $\Delta\rho = 0.1 \text{ kgm}^{-3}$ and thickness of about 15 m
405 (i.e. allowed some dilution and increase in thickness due to entrainment), a very crude
406 estimate of the Froude number ($Fr = 0.25$) will yield an entrainment coefficient of about
407 $E = 6 \times 10^{-5}$ [Fernando, 1991]. This will roughly double the plume volume over the 11
408 days it takes to reach the deep basin, i.e. 4 times flushing will suffice to account for the
409 volume below the sill. Acting over the mean polynya width of 50 km, the total mean
410 volume flux (BSW plus the entrainment) yields a filling time of 14 days. We can then
411 estimate about 25 days (downflow time plus the filling time) from the start of the freezing
412 period to the start of weak overflow at the sill. A significant polynya event will then cause
413 a pulse which will propagate as an interfacial wave and reach the sill in one to three days.

414 Note that each of the 130 polynya flushing events carried an approximate volume of
415 $1.4 \times 10^{10} \text{ m}^3$ after entrainment when it reached the deep basin. Removing 4 events needed
416 to fill the basin, this yields a total volume transport at the sill of about 0.06 Sv over one
417 year. This rough estimate of the annual overflow transport is consistent with previous
418 observations [Schauer, 1995] and recent monitoring results at the Storfjorden sill [Fer,
419 2007].

420 The CTD section in the vicinity of the sill (Figure 8) was occupied approximately
421 22 days after the supercooling event and 15 days after the completion of the polynya
422 hydrography survey (Figure 6). BSW overflow is detected with potential temperature

423 <-1.9 °C and salinity of ~ 35.2 , consistent with the BSW characteristics in the polynya
424 (Figure 4). Approximately 12 days after the first cast in the polynya, a high-salinity front
425 flowed past the sensors on the bottom-mounted ADCP frame at the sill (arrow in Figure
426 9a). Based upon the above scaling, we hypothesize that this is the signature at the sill
427 in response to a significant polynya event. The CTD survey and the time series at the
428 sill suggest a lag of 12 to 18 days between the supercooling event and the pulse in the
429 overflow, which is consistent with the conservative analytical estimate. The 12-18 days
430 lag is also a conservative estimate as the polynya event could have started prior to our
431 first CTD cast.

432 In order to test our hypothesis the following idealized numerical simulation is con-
433 ducted using the Bergen Ocean Model (BOM) [Berntsen and Svendsen, 1999; Berntsen,
434 2000, 2002] forced with wind generated using the limited-area, non-hydrostatic, sigma-
435 coordinate model MM5 [Dudhia, 1993]. The model setup is similar to that in Skogseth
436 et al. [2007b] where climatological values of velocity, temperature, salinity and surface ele-
437 vation [Engedahl et al., 1998], are interpolated onto the model grid and are used as initial
438 values. The hydrographical archive contains gridded hydrographical data originating from
439 the databases of Levitus [1982] and Damm [1989] as well as observations. Initially, BSW
440 is absent in the basin (Figure 13a). As BOM lacks an ice component, the polynya and
441 the ice cover is approximated as follows: 1) An artificial polynya was positioned where
442 the Storfjorden polynya recurs each year. 2) The mean polynya area, surface heat and
443 salinity fluxes are prescribed using the winter 1999 results of the polynya model reported
444 in [Skogseth et al., 2004]. Winter 1999 is a moderate brine production year comparable to
445 winter 2006 (Section 4.1). 3) Assuming that the ice cover prevents wind from acting on

446 the ocean surface, the wind forcing was only applied to the ice-free areas, i.e., the polynya
447 and west of the shelf break of the western Barents Sea.

448 Modeled downflow of dense polynya water started on Day 8 as a tongue of dense water
449 at about 77.5° N and 20.5° E (64 km southwest of Station 16) underneath the designated
450 polynya area (dark red color in Figure 13). Downflow was weaker in the observation site
451 close to Kapp Lee. The BSW downflow continued, concentrated at these sites, growing
452 broader and thicker, and eventually filled the basin to the sill level by Day 29, initiating
453 an overflow (Figure 13b). The signature of the dense BSW produced in the polynya
454 thus arrives in about 20 days to the sill. This is comparable to the estimate from the
455 observations and the analytical analysis. The BSW production at the polynya exceeds
456 the volume flux of the dense overflow at the sill, which is possibly constrained by rotational
457 effects, by Day 56, Storfjorden was filled to the submarine ridge level at 80 m depth (at
458 about 77.25° N and 18.5° E, see Figure 1 for location) and spilled across the ridge.

4.5. Overflow Plume Width in Winter

459 Two moorings situated ~ 40 km downstream of the sill indicated an overflow width less
460 than 15 km in 1992 and 1994 [Schauer, 1995; Schauer and Fahrback, 1999]. Existing
461 transport estimates of the overflow were therefore made using a typical plume width of 15
462 km. Observations reported here suggest that this can be an underestimate in winter. The
463 CTD section in Figure 8 shows a BSW plume with ~ 30 m thickness at the eastern edge
464 of the sill (Station 48). Under rotational control, the plume leans towards the west wall
465 of the sill looking downstream, hence we conclude that the overflow most likely occurred
466 across the entire sill width of ~ 40 km. CTD sections at the sill in summer and autumn
467 from 1999 to 2002 have revealed overflow of BSW remnants with a width of 15-20 km

468 from the western edge of the sill [Skogseth et al., 2005b; Fer et al., 2004b]. Assuming that
469 the overflow is independent of the tidal cycle, our observations indicate that the overflow
470 cross-section at the sill is larger in the freezing period than in summer and autumn.

4.6. Effects of Eddies

471 The rise in the isopycnals observed between Stations 8 and 10 (Figure 6b) is connected
472 with the ongoing brine release and downflow, and it has the structure of a small eddy.
473 The dome covers about 60% of the 30 m water column and appears nearly uniform in
474 density between 5 and 25 m. The dome might be caused by processes including topo-
475 graphically enhanced tidal currents, eddies caused by the conservation of potential energy
476 over steep topography, eddies triggered by instabilities along the polynya front, converg-
477 ing topographically steered currents, and spatial variability in wind stress. Numerical
478 model [Gawarkiewicz and Chapman, 1995] and laboratory studies [Cenedese et al., 2004]
479 indicate that eddy activity at the density front controls the downflow of dense water from
480 the shallow shelves. Observations from densely spaced moorings in the St. Lawrence
481 polynya have not detected eddies that might lead to such cross-shelf exchange [Danielson
482 et al., 2006]. Albeit inconclusive due to undersampling and lack of current measurements,
483 present observations of downflow of newly formed BSW from the shallow polynya area,
484 following a supercooling event, indicate that the downflow was connected to a doming in
485 the pycnocline in the vicinity of the steepest topography (Figure 6), which might indicate
486 eddy activity along the polynya edge.

4.7. Storfjordbanken as a Site for BSW Production and Downflow

487 The shallow Storfjordbanken on the eastern slope of the fjord (Figure 1) is a potential
488 candidate for BSW production and polynya activity, but observations are scarce. The
489 CTD section off Storfjordbanken east of the sill (Figure 7) indicates no downflow of BSW
490 from the shallow bank area south of the sill towards Storfjordrenna. CTD sections ob-
491 tained in March 2003 from R.V. Polarstern also lack BSW downflow in this area [Fer
492 et al., 2004a]. The only indication of BSW downflow from the shallow areas was found
493 in the northernmost sections closest to the west coast of Edgeøya. The most likely expla-
494 nation is that the polynya activity is most frequent with longer duration along the west
495 coast of Edgeøya than around Tusenøyane on Storfjordbanken south of Edgeøya. This
496 is also consistent with the results on persistent polynya areas during the winter of 2000
497 [Smedsrud et al., 2006]. Earlier model studies revealed topographically enhanced tidal
498 currents in an anticyclonic sense on Storfjordbanken [Skogseth et al., 2007b], which might
499 confine the dense water on the shallow bank.

500 The idealized model results also suggest that the shallow polynya area south of Edgeøya
501 near Storfjordbanken is not effective in BSW downflow despite the ice production (Fig-
502 ure 13). The topography guides the dense water effectively northwards along the slope,
503 consistent with lack of BSW downflow signature off Storfjordbanken in this study (Figure
504 7) and for March 2003 [Fer et al., 2004a]. Our model results thus complement the scarce
505 data and we conclude that Storfjordenbanken is not an effective BSW downflow site. The
506 produced BSW is topographically confined to the bank and advected into Storfjorden for
507 further densification.

5. Summary and Conclusions

508 During two field experiments in April 2004 and 2006, hydrographical and current data
509 were collected in the active Storfjorden polynya. Production and downflow of BSW from
510 shallow areas to the deeper basin inside Storfjorden are documented herein.

511 During a period of strong heat loss and intense frazil ice growth in the Storfjorden
512 polynya in April 2006, the BSW salinity exceeded 35.3. The shallow near-shore areas in
513 Storfjorden are effective and important brine production sites, and are able to increase
514 density locally by as much as 0.5 kgm^{-3} . Major portions of the BSW in April 2006 had a
515 salinity of ~ 35.1 , comparable to earlier observations, and was $\sim 0.15 \text{ kgm}^{-3}$ denser than
516 the local surface water.

517 Despite the large ice production in winter 2004 (twice that in 2006), and comparable
518 densification of 0.15 kgm^{-3} , the BSW salinity was less than 34.8. This is a consequence
519 of relatively fresh source water. Anomalously fresh surface water existed in the western
520 Barents Sea in spring and summer 2003, consistent with heavy ice conditions the previous
521 winter.

522 Strong tides, offshore wind and currents keep the polynya on the eastern shores of Stor-
523 fjorden frequently open, in contrast with the deeper areas of the fjord. The BSW downflow
524 close to Edgeøya was most significant where the bathymetry was steepest, confirming both
525 the idealized numerical model study and analytical estimates of such downflow. The model
526 results suggest the strongest downflow to be directly west of Edgeøya at $77^\circ 30' \text{ N}$, which
527 is suggested here as a key area for monitoring the downflow. Downflow of BSW from the
528 shallow Storfjordbanken was absent both in observations and the model results.

529 Inferred from observations, winter-time extent of the BSW overflow plume covers the
530 entire sill of about 40 km. This is much greater than 15 km which is typically used in

531 transport calculations. Current, salinity and temperature data in the core of the overflow
532 at the sill indicate a time lag of 12-18 days from the observed maximum salinity and
533 downflow in the polynya area to overflow with similar characteristics at the sill. This
534 downflow-overflow link is confirmed by an idealized numerical model and theoretical cal-
535 culations.

536 The BSW downflow is guided by the complex bathymetry in Storfjorden. High resolu-
537 tion hydrographical data are needed to capture the downflow, and model studies have to
538 implement fine-grid bathymetric data with resolution of 0.5-1 km to properly resolve such
539 flow. One of our sections inside the polynya indicates an eddy like feature of 2 km width.
540 Such eddies and instabilities in the polynya may be an important signature of cascading
541 and downflow.

542 Freemansundet influences the polynya dynamics. Here, strong currents up to 53 cm s^{-1}
543 are dominated by the M_2 tidal wave. Shallow water tides (M_4 and M_6) are observed and
544 reflects the nonlinear interaction of M_2 when the tidal wave propagates through the shallow
545 sound. The presence of an ice cover and the shallow depth in Freemansundet introduces
546 boundary effects, whereby the residual current veers to the right toward the upper (ice)
547 and lower (bottom) boundaries. In April 2004 a net transport of 0.05 Sv less saline and
548 warmer water into Storfjorden from the northwestern Barents Sea was measured, probably
549 controlled by the wind direction and corresponding Ekman transport. The complex tidal
550 pattern mixes such source water effectively.

551 Storfjorden is one of the important BSW production sites in the Arctic. In the same
552 way as other polynyas of the Arctic, the Storfjorden polynya releases salt effectively, and
553 makes the underlying water denser than the source water in the range $0.15 - 0.5 \text{ kg m}^{-3}$,

554 depending on atmospheric forcing. Subsequent downflow depends on this density increase
555 and topography. The density and volume of the final overflow reaching the deep ocean
556 are thus also dependant and sensitive to the source water.

557 **Acknowledgments.** This work was conducted as a part of the Polar Ocean Climate
558 Processes project (PROCLIM) funded by the Norwegian Research Council, through Grant
559 155923/700. We want to acknowledge the logistic department at UNIS, the Governor on
560 Svalbard, Airlift and the crew on the coastguard K/V Svalbard for great support and
561 service. We are grateful to Stefan Claes and Jon Jeppesen for help during the fieldwork,
562 Anne Dagrund Sandvik for the wind stress fields from MM5, Lars Asplin for support to
563 the model set-up with BOM, our project manager Peter M. Haugan and two anonymous
564 reviewers for valuable comments. This is publication nr. A184 from the Bjerknes Centre
565 for Climate Research.

References

- 566 Aagaard, K., L. K. Coachman, and E. Carmack: 1981, On the halocline of the Arctic
567 Ocean. *Deep Sea Res., Part A*, **28**, 529–545.
- 568 Anderson, L. G., E. P. Jones, R. Lindgren, B. Rudels, and P.-I. Sehlstedt: 1988, Nutrient
569 regeneration in cold, high salinity bottom water of the Arctic shelves. *Cont. Shelf Res.*,
570 **8**, 1345–1355.
- 571 Berntsen, J.: 2000, Users guide for a modesplit σ -coordinate numerical ocean model
572 version 1.0. Report 135, Department of Applied Mathematics, University of Bergen,
573 Bergen, Norway.

- 574 — 2002, Internal pressure errors in sigma-coordinate ocean models. *J. Atmosph. and*
575 *Ocean. Techn.*, **19**, 1403–1414.
- 576 Berntsen, J. and E. Svendsen: 1999, Using the Skagex dataset for evaluation of ocean
577 model skills. *J. Mar. Sys.*, **18**, 313–331.
- 578 Cavalieri, D. J. and S. Martin: 1994, The contribution of Alaskan, Siberian, and Canadian
579 coastal polynyas to the cold halocline layer of the Arctic Ocean. *J. Geophys. Res.*, **99**,
580 18,343–18,362.
- 581 Cenedese, C., J. Marshall, and J. A. Whitehead: 2004, A laboratory model of thermocline
582 depth and exchange fluxes across circumpolar fronts. *J. Phys. Oceanogr.*, **34**, 656–667.
- 583 Damm, P.: 1989, Klimatologischer Atlas des Salzgehaltes, der Temperatur und der Dichte
584 in der Nordsee, 1968-1985. Technical Reports 89-6, Institut für Meereskunde, Hamburg.
- 585 Danielson, S., K. Aagaard, T. Weingartner, S. Marin, P. Winsor, and G. Gawarkiewicz:
586 2006, The St. Lawrence polynya and the Bering shelf circulation: New observations and
587 a model comparison. *J. Geophys. Res.*, **111**, doi:10.1029/2005JC003268.
- 588 Drucker, R., S. Martin, and R. Moritz: 2003, Observations of ice thickness and frazil ice
589 in the St. Lawrence Island polynya from satellite imagery, upward looking sonar, and
590 salinity/temperature moorings. *J. Geophys. Res.*, **108**, C5, doi:10.1029/2001JC001213.
- 591 Dudhia, J.: 1993, A nonhydrostatic version of the Penn State/NCAR mesoscale model:
592 Validation tests and simulation of an Atlantic cyclone and cold front. *Mon. Wea. Rev.*,
593 **121**, 1493–1513.
- 594 Engedahl, H., B. Ådlandsvik, and E. Martinsen: 1998, Production of monthly mean
595 climatological archives for the Nordic Seas. *J. Mar. Sys.*, **14**, 1–26.
- 596 Fer, I.: 2006, Scaling turbulent dissipation in an Arctic fjord. *Deep-Sea Res. II*, **53**, 77–95.

- 597 — 2007, Current measurements at the storfjorden sill, 2004 - 2006. Technical Report 1,
598 Reports in Meteorology and Oceanography, Geophysical Institute, University of Bergen.
- 599 Fer, I., I. Harms, T. Martin, S. Pisarev, B. Rudels, U. Schauer, and A. Sirevaag: 2004a,
600 Water masses and circulation: Shelf convection in the western Barents Sea and Atlantic
601 water north of Svalbard. *The Expedition ARKTIS XIX/1 a, b and XIX/2 of the Research*
602 *Vessel "POLARSTERN" in 2003*, U. Schauer and G. Kattner, eds., Alfred-Wegener-
603 Institut für Polar- und Meeresforschung, Bremerhaven, Bundesrepublik Deutschland,
604 volume 481 of *Berichte zur Polar- und Meeresforschung*, chapter 5, 72–87.
- 605 Fer, I., U. Lemmin, and S. A. Thorpe: 2002, Winter cascading of cold water in Lake
606 Geneva. *J. Geophys. Res.*, **107**, doi: 10.1029/2001JC000828.
- 607 Fer, I., R. Skogseth, and P. M. Haugan: 2004b, Mixing of the Storfjorden (Svalbard
608 Archipelago) overflow inferred from density overturns. *J. Geophys. Res.*, **109**, C01005,
609 doi:10.1029/2003JC001968.
- 610 Fer, I., R. Skogseth, P. M. Haugan, and P. Jaccard: 2003, Observations of the Storfjorden
611 overflow. *Deep-Sea Res. I*, **50**, 1283–1303.
- 612 Fernando, H. J. S.: 1991, Turbulent mixing in stratified flows. *Annu. Rev. Fluid Mech.*,
613 **23**, 455–493.
- 614 Gawarkiewicz, G. and D. C. Chapman: 1995, A numerical study of dense water formation
615 and transport on a shallow, sloping continental shelf. *J. Geophys. Res.*, **100**, 4489–4508.
- 616 Haarpaintner, J., J. C. Gascard, and P. M. Haugan: 2001, Ice production and brine
617 formation in Storfjorden, Svalbard. *J. Geophys. Res.*, **106**, 14,001–14,013.
- 618 Haas, C., J. Lieser, J. Lobach, T. Martin, A. Pfaffling, S. Willmes, V. Alexandrov,
619 and S. Kern: 2004, Sea ice physics. *The Expedition ARKTIS XIX/1 a, b and XIX/2*

620 of the Research Vessel "POLARSTERN" in 2003, U. Schauer and G. Kattner, eds.,
621 Alfred-Wegener-Institut für Polar- und Meeresforschung, Bremerhaven, Bundesrepub-
622 lik Deutschland, volume 481 of *Berichte zur Polar- und Meeresforschung*, chapter 3,
623 13–46.

624 Killworth, P. D.: 2001, On the rate of descent of overflows. *J. Geophys. Res.*, **106**,
625 2226722275.

626 Kwok, R., W. Maslowski, and S. W. Laxon: 2005, On large outflows of Arctic sea ice into
627 the Barents Sea. *Geophys. Res. Lett.*, **32**, L22503, doi:10.1029/2005GL024485.

628 Levitus, S.: 1982, Climatological atlas of the world ocean. *NOAA Prof. Pap.*, **13**, 1–173.

629 Maus, S.: 2003, Interannual variability of dense shelf water salinities in the north-western
630 Barents Sea. *Pol. Res.*, **22**, 59–66.

631 Nof, D.: 1983, The translation of isolated cold eddies along a sloping bottom. *Deep-Sea*
632 *Res.*, **30**, 171–182.

633 Pawlowicz, R., B. B., and L. S.: 2002, Classical tidal harmonic analysis including error
634 estimates in MATLAB using T_TIDE. *Computers and Geosciences*, **28**, 929–239.

635 Quadfasel, D., B. Rudels, and K. Kurz: 1988, Outflow of dense water from a Svalbard
636 fjord into the Fram Strait. *Deep-Sea Res.*, **35**, 1143–1150.

637 Rudels, B. and D. Quadfasel: 1991, Convection and deep water formation in the Arctic
638 Ocean-Greenland Sea system. *J. Mar. Sys.*, **2**, 435–450.

639 Schauer, U.: 1995, The release of brine-enriched shelf water from Storfjord into the Nor-
640 wegian Sea. *J. Geophys. Res.*, **100**, 16,015–16,028.

641 Schauer, U. and E. Fahrbach: 1999, A dense bottom water plume in the western Barents
642 Sea: Downstream modification and interannual variability. *Deep-Sea Res. I*, **46**, 2095–

2108.

Shapiro, G. I., J. M. Huthnance, and I. V. V.: 2003, Dense water cascading off the continental shelf. *J. Geophys. Res.*, **108**, doi:1029/2002JC001610.

Shcherbina, A. Y., L. D. Talley, and D. L. Rudnick: 2004, Dense water formation on the northwestern shelf of the Okhotsk Sea: 1. direct observations of brine rejection. *J. Geophys. Res.*, **109**, C09S08, doi:10.1029/2003JC002196.

Skogseth, R., I. Fer, and P. M. Haugan: 2005a, *The Nordic Seas An Integrated Perspective*, AGU, volume 158 of *Geophysical Monograph Series*, chapter Dense-water production and overflow from an Arctic coastal polynya in Storfjorden. 73–88.

Skogseth, R., P. M. Haugan, and J. Haarpaintner: 2004, Ice and brine production in Storfjorden from four winters of satellite and in situ observations and modeling. *J. Geophys. Res.*, **109**, C10008, doi:10.1029/2004JC002384.

Skogseth, R., P. M. Haugan, and M. Jakobsson: 2005b, Watermass transformations in Storfjorden. *Cont. Shelf Res.*, **25**, 667–695.

Skogseth, R., F. Nilsen, and L. H. Smedsrud: 2007a, Observations of in-situ supercooled water in an Arctic polynya. *Geophys. Res. Let.*, Submitted.

Skogseth, R., A. L. Sandvik, and L. Asplin: 2007b, Wind and tidal forcing on the meso-scale circulation in Storfjorden, Svalbard. *Cont. Shelf Res.*, **27**, 208–227, doi:10.1016/j.csr.2006.10.001.

Smedsrud, L. H., W. P. Budgell, A. D. Jenkins, and B. Ådlandsvik: 2006, Fine scale sea ice modelling of the Storfjorden polynya. *Annals of Glaciology*, **44**, 73–79.

Smedsrud, L. H. and R. Skogseth: 2006, Field measurements of Arctic grease ice properties and processes. *Cold Reg. Sci. Techn.*, **44**, 171–183.

⁶⁶⁶ Wålin, A. K.: 2004, Topographic advection of dense bottom water. *J. Fluid. Mech.*, **510**,
⁶⁶⁷ 95–104.

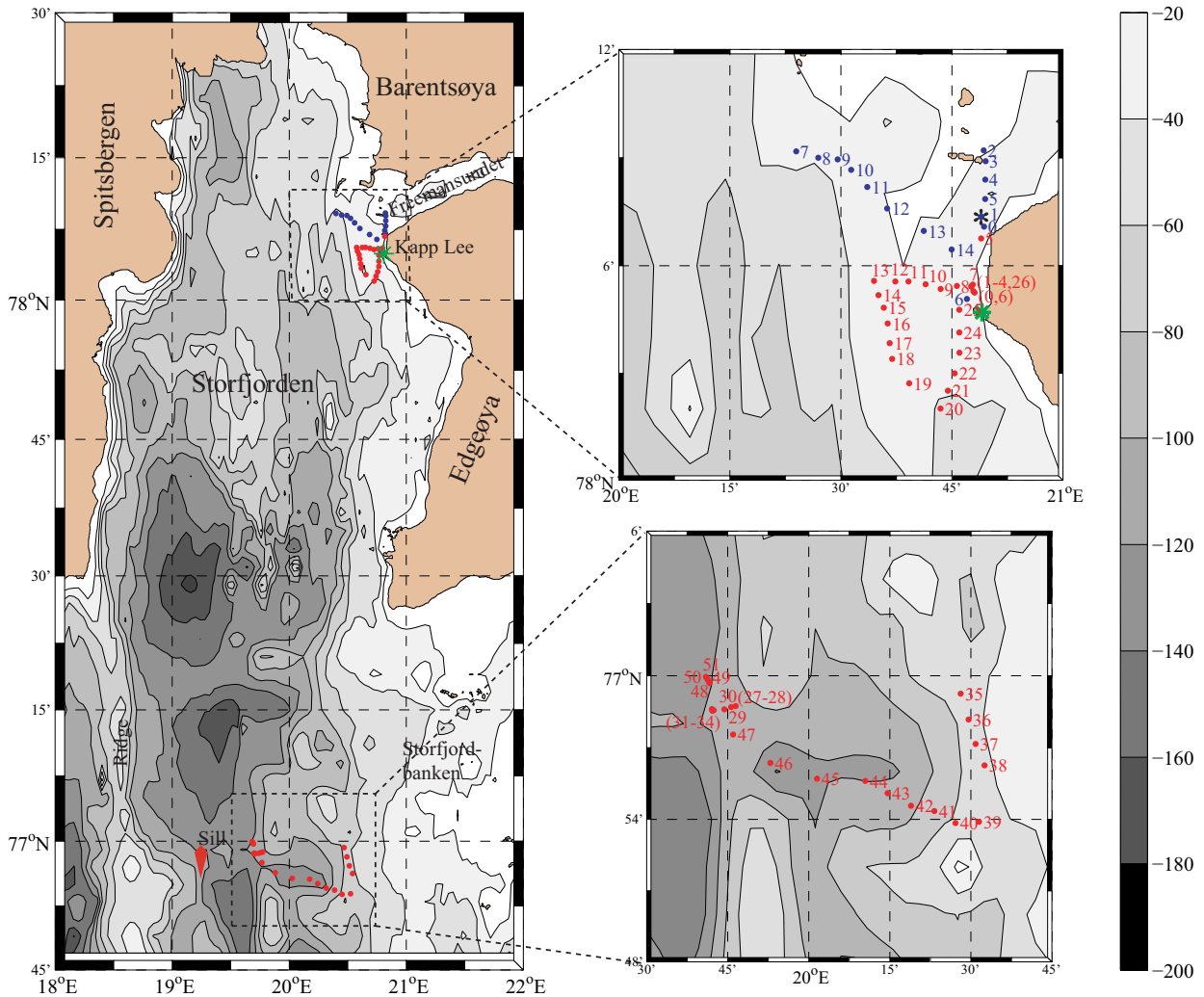


Figure 1. Storfjorden surrounded by the islands Spitsbergen, Barentsøya and Edgeøya in the Svalbard Archipelago. Kapp Lee on Edgeøya is indicated, and the CTD stations are marked with blue (April 2004) and red (April 2006) dots and numbers. The dashed boxes on the large map indicate the borders of the close-up maps. The meteorological station on Kapp Lee, the RDCP station in Freemansundet and the ADCP at the sill are indicated with a green star, a black star and a red diamond, respectively. The depth contours are in meters.

D R A F T

February 4, 2008, 11:32pm

D R A F T

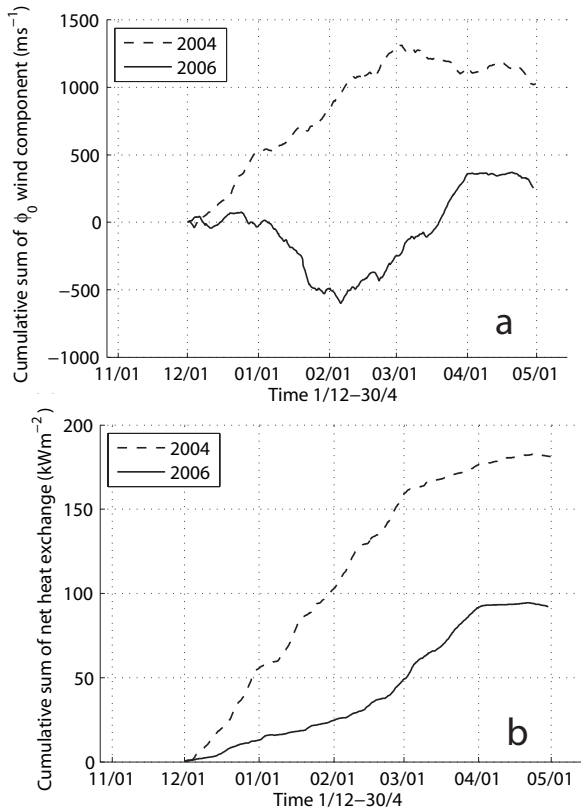


Figure 2. The cumulative sum of a) wind velocity in the favorable direction and b) total heat loss (b) for the freezing seasons 2004 and 2006. In situ meteorological data from Hopen Island are adjusted for Storfjorden as described in Skogseth et al. [2004].

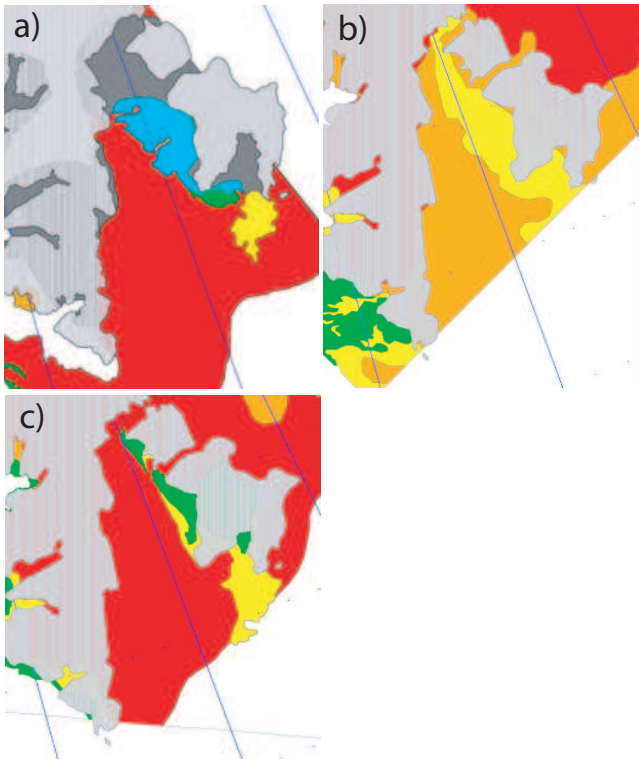


Figure 3. Ice charts over Storfjorden on a) April 14 2004, b) April 4 2006 and c) April 18 2006, where dark gray is fast ice, red is very close drift ice, orange is close drift ice, yellow is open drift ice, green is very open drift ice and blue is open water. The ice charts are available on http://polarview.met.no/cgi-bin/highres_arkiv.pl and are delivered by Norwegian Ice Service at met.no financed through the ESA GMES funded project Polarview and Norwegian Space Centre.

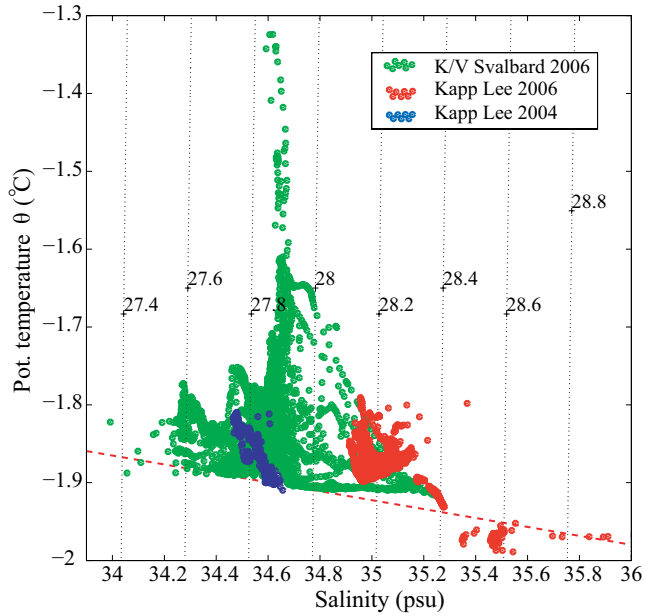


Figure 4. Potential temperature and salinity plot of the CTD-profiles in Storfjorden outside Kapp Lee in April 2004 (blue) and March-April 2006 (red), and in the vicinity of the sill in April 2006 (green). Density (σ_θ) lines every 0.2 kgm^{-3} are drawn, and the freezing point temperature referred to surface is indicated by the red stippled line.

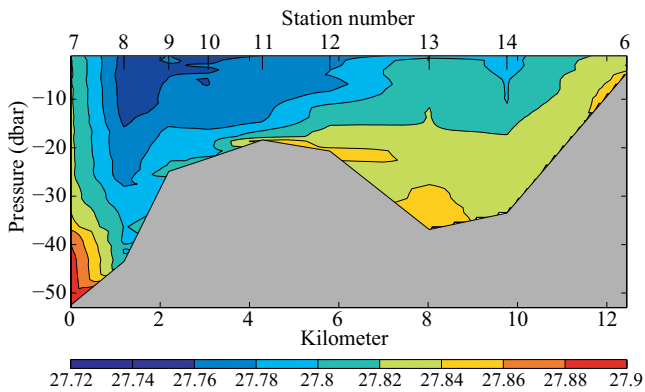


Figure 5. Section of isopycnals (σ_θ) from the CTD stations in Storfjorden outside Kapp Lee in April 2004. Contour interval is 0.02 kgm^{-3} . For station locations see Figure 1.

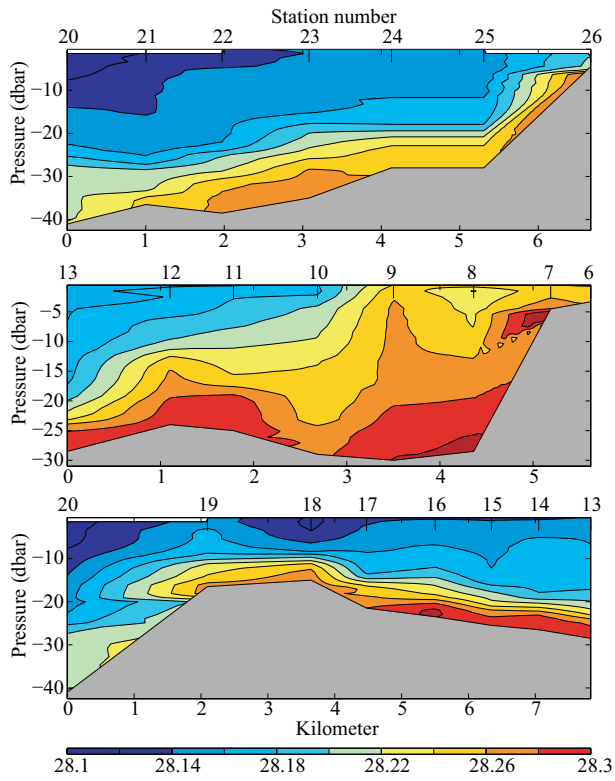


Figure 6. Sections of isopycnals (σ_θ) from the CTD stations in Storfjorden outside Kapp Lee in April 2006. Contour interval is 0.02 kgm^{-3} . For section and station locations see Figure 1.

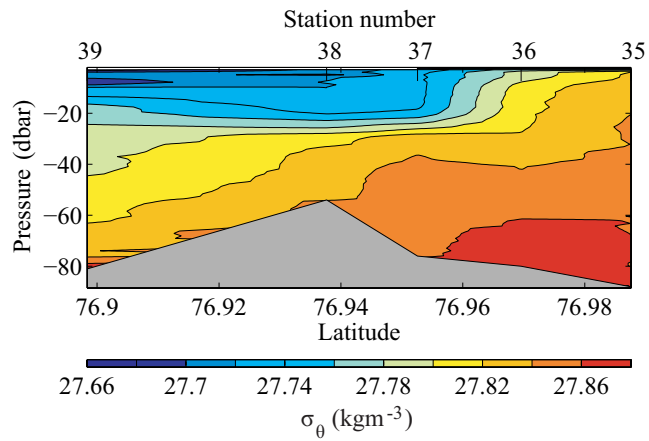


Figure 7. Section of isopycnals (σ_θ) from the CTD stations off Storfjordbanken south of the sill in Storfjorden in April 2006. Contour interval is 0.02 kgm^{-3} . For section and station locations see Figure 1.

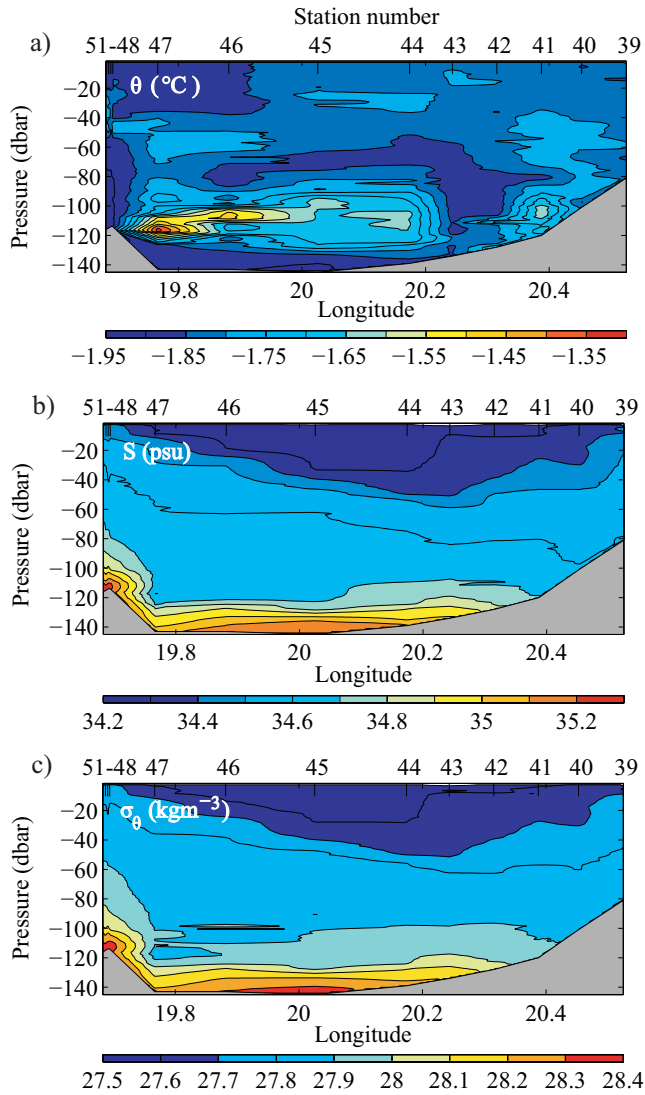


Figure 8. Sections of a) isothermals, b) isohalines and c) isopycnals (σ_{θ}) from the CTD stations in the vicinity of the sill in Storfjorden in April 2006, where θ -, S- and σ_{θ} -lines every 0.05 $^{\circ}\text{C}$, 0.1 psu and 0.1 kgm^{-3} are drawn and indicated in the colorbars, respectively. For section and station locations see Figure 1.

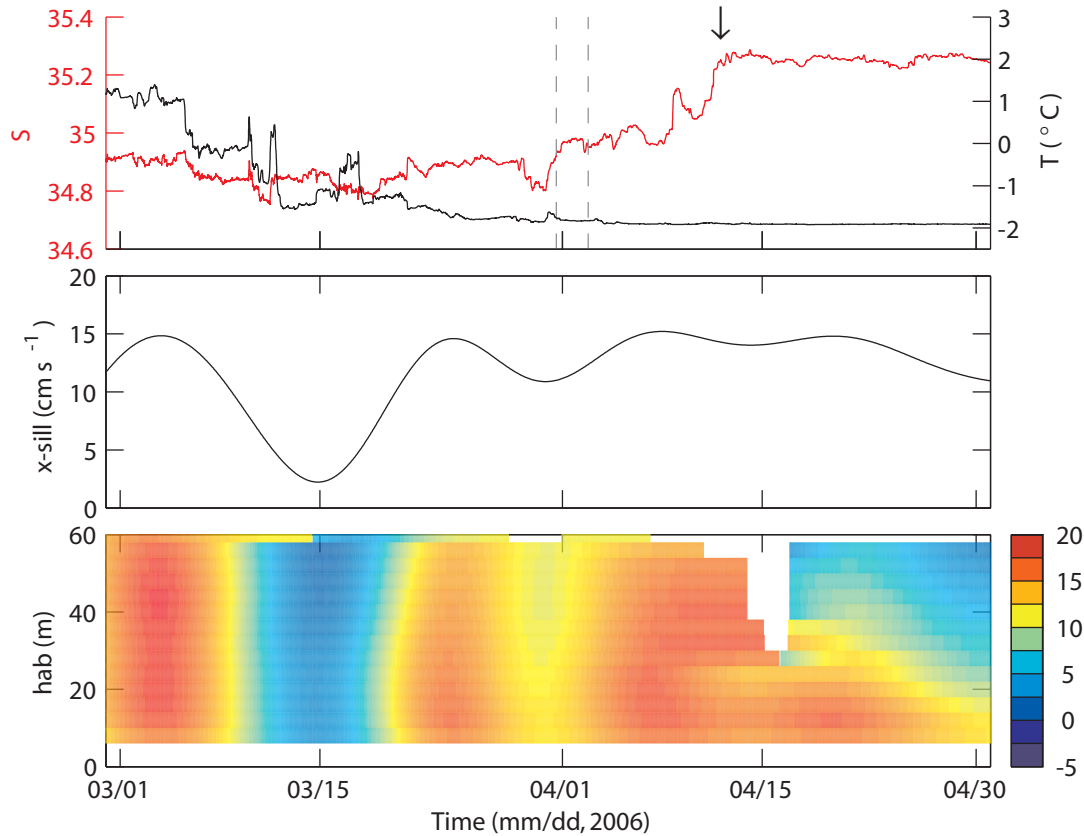


Figure 9. Time series derived from the bottom-mounted ADCP and Microcat deployed at the Storfjorden sill (Figure 1). a) 10-minute sampled bottom (black) temperature and (red) salinity. Vertical dashed lines mark the time of the first and the last CTD cast when supercooling was observed. The arrow marks the time of passage of the first high-salinity front after the supercooling event. b) Cross-sill component of the velocity recorded at the bottom-most depth bin, 6 m height above bottom (hab). c) Time-hab map of cross-sill component of velocity. 10-minute current profiles are hourly averaged and 15-day low-pass filtered. White portions in c) are times with poor data quality after screening, largely due to lack of scatters. Noisy features away from the bottom are portions of data not sufficiently long enough for 15-days filtering.

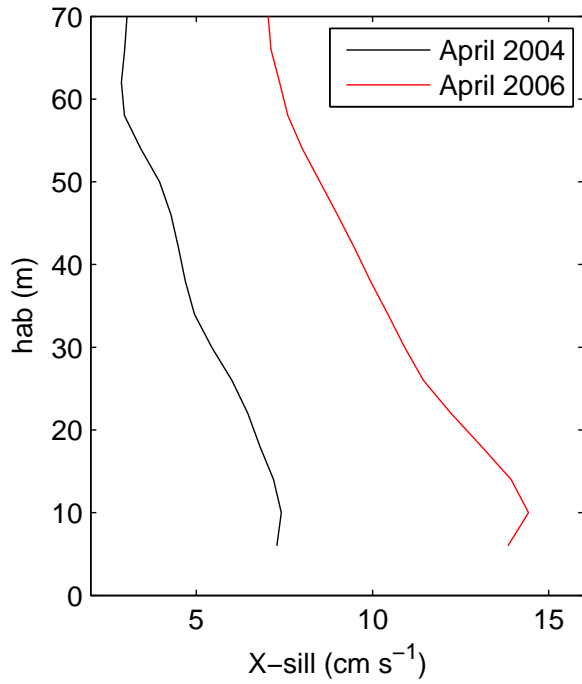


Figure 10. Profiles of the cross-sill component of the velocity measured at the Storfjorden sill. Profiles are averages for (black) April 2004 and (red) April 2006.

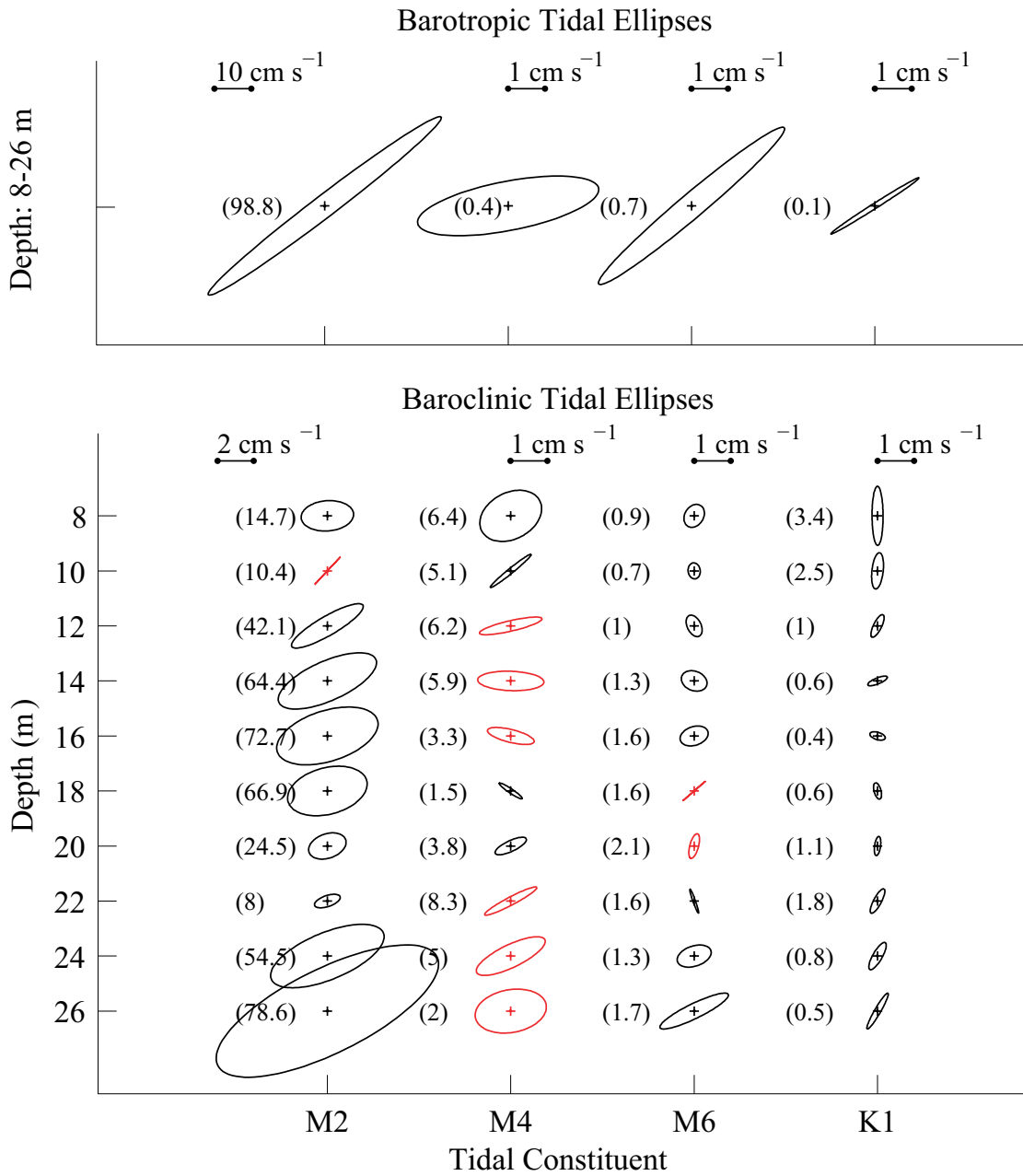


Figure 11. The barotropic and baroclinic tidal ellipses derived from the RDCP deployed at Freemansundet from April 18 to 21 2004 as a function of depth, for M₂, M₄, M₆ and K₁, with scales indicated. The sense of rotation is clockwise for black and counterclockwise for red ellipses. Numbers in brackets are percent of variance explained in the barotropic and baroclinic currents at each depth bin, for the corresponding constituent.

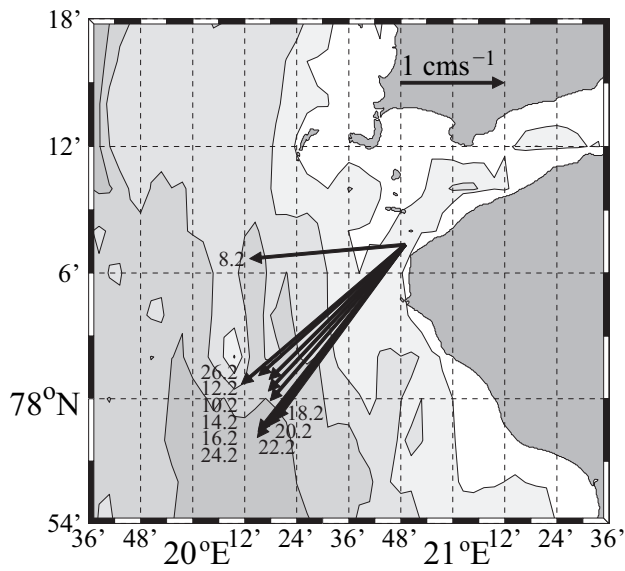


Figure 12. Mean residual current vectors in Freemansundet estimated from the RDCP data from April 18 to 21 2004 at a 2 m interval between 8.2 m and 26.2 m depths. Numbers indicated close to the arrowheads are the respective depths in m. Tides are filtered.

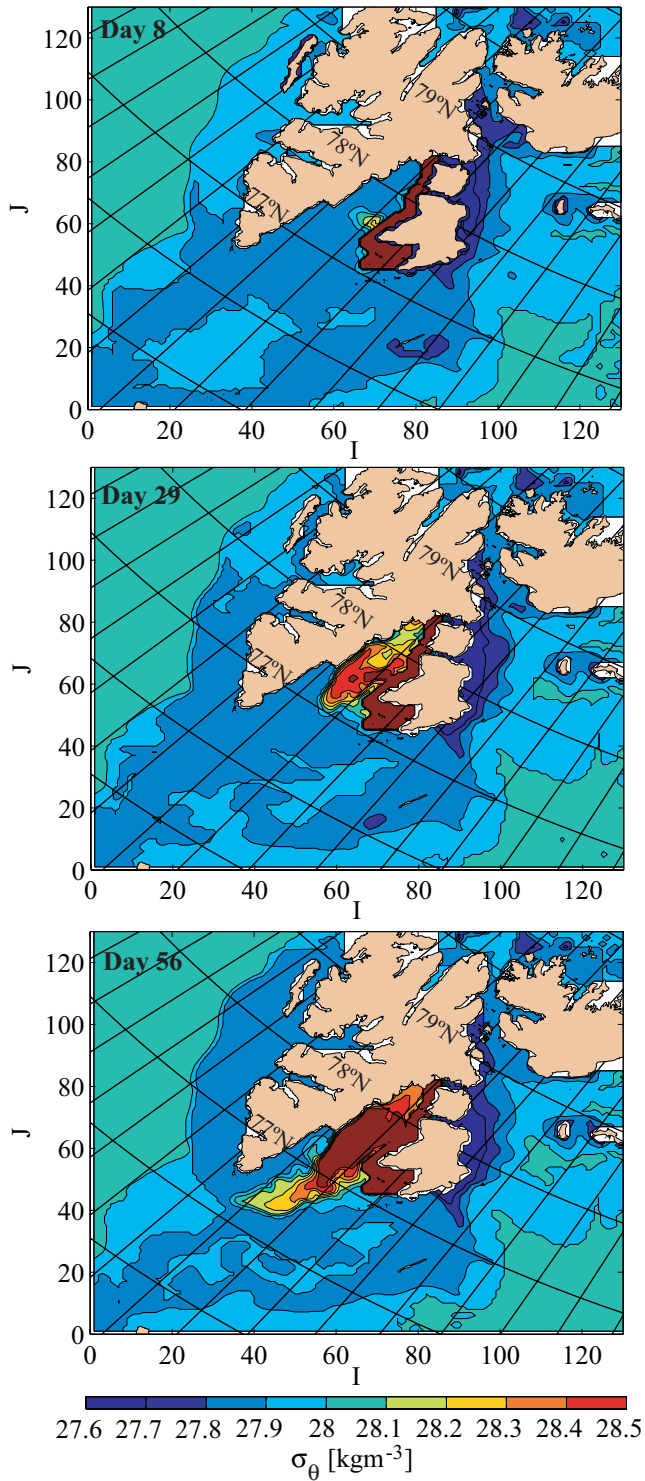


Figure 13. Modelled isopycnals (σ_θ) along the bottom from the BOM simulation forced with salt and heat flux representing the approximate effects of the Storfjorden polynya in winter 1998/1999 after 8, 29 and 56 days of simulation. Isopycnals are drawn at 0.1 kgm^{-3} intervals.